PAPER Nr.: 48

AEROELASTIC MODELLING OF WIND TURBINE ROTORS

BY

H. SNEL

NETHERLANDS ENERGY RESEARCH FOUNDATION ECN
PETTEN, THE NETHERLANDS

FIFTEENTH EUROPEAN ROTORCRAFT FORUM

SEPTEMBER 12 - 15, 1989 AMSTERDAM

AEROELASTIC MODELLING OF WIND TURBINE ROTORS

by

H. Snel
Netherlands Energy Research Foundation ECN
Postbus 1
1755 ZG Petten
The Netherlands

Abstract

In the design of modern large scale wind turbines, aeroelastic effects play an important role. Rotor blades made out of GRP materials have considerable flexibility. Oftentimes flexible elements are introduced on purpose, to limit load fluctuations. Aeroelastic stability and tuning than becomes a major point of concern in the design of the blade.

At ECN, work is in progress in the field of numerical simulation of the dynamic behaviour of wind turbine blades. The modelling of the structural dynamics of the blades is the subject of the present paper.

The blades are modelled as slender beams, with non-uniform mass and elasticity distributions. The motion of the blades is described by the full non-linear partial differential equations of the rotating and elastically deforming rotor. These equations are solved using finite difference techniques, and cubic spline approximations for the deformation field. The cubic spline yields a very good approximation as it contains the physical characteristics of the deformed blade: derivatives up to second order (related to the bending moments) are continuous. The time finite difference is chosen to be implicit, in order to obtain favourable stability characteristics.

The model and the solution method will be explained in some detail. Sample calculations will be shown, and compared with measurements.

1. Introduction

Modern wind turbines constitute complex dynamical systems. Apart from the basic degree of freedom (dof) of solid body rotation about the rotor axis, many other dof's are present. Tower top motion due to tower flexibility, yawing, a teeter hub, form other solid body type dof's for the rotor. The rotor blades, frequently constructed in GRP materials, undergo important elastic deformations. Oftentimes, flexibilities are used on purpose by the wind turbine designer in order to ameliorate loads and, especially, load fluctuations.

At the same time, the input to the system is very complex. Wind turbulence causes exitations in a wide range of frequencies, higher frequencies entering mainly due to the rotation of the blades through turbulent structures of size smaller than the rotor diameter. Moreover, harmonic (with respect to the basic rotational frequency) excitations are present as a result of the tower disturbance and gravita-

tion. In variable rotor speed systems (used both for higher energy yield as for the reduction of load fluctuations), the excitations and system eigenfrequencies may cover a large range of frequencies.

Although many similarities are present with helicopter rotor dynamics, there are also important differences, such as the gravitational and tower effects. Since the tip speed ratio $\Omega R/U_w$ of a wind turbine covers a wide range of values, linearization of the aerodynamics is not warranted. Also, structural non-linearities may be significant, an important example being Coriolis couplings. Hence the system should be treated as non-linear.

To avoid instabilities, or high load factors, careful tuning of the system in the design phase is necessary. Computer codes, simulating the system, are being developed at several institutes to serve as design tools and for certification purposes. The present paper concentrates on the modelling of the dynamics, especially of flexible blades, as used in the ECN-PHATAS code. Also, the numerical methods used to solve the resulting equations, will be discussed. Since the system is non-linear, the simulation will be done in the time domain. Of course, subsequent frequency analysis of the calculated signal may be very helpful.

2. Modelling of blade flexibility

Blade flexibility can be realized structurally in various ways, such as:

i) hinges, with or without springs and dampers. Sometimes coupled in the form of a teeter hinge.
ii) flexbeams: highly flexible parts at the blade-hub attachment.
iii) continuously distributed elasticity over the entire blade span.

Combinations of the above are also used.

In some codes, continuous forms of deformation, (ii) or (iii) are modelled by way of hinges and springs, such that the basic eigenfrequencies and their dependence on the rotational speed (Southwell coefficients) are correctly represented. However, a fundamental problem arises when flexibility in more than one direction is present. One has to decide upon a hinge sequence, e.g. flap torsion or torsion flap. Either option will give a different type of deformation, which at best will only be a reasonable approximation of reality. Moreover, it will not be possible to obtain the correct rate of deformation at all radial positions even if the basic eigenfrequency is correctly modelled by the hinge. This will result in deficient prediction of aerodynamic damping, and consequently of stability limits or limit cycle amplitudes.

For these reasons, blade flexibility (apart from a possible teeterhinge) is modelled here in terms of continuous distributions of mass and elasticity properties, along the blade axis. The dynamical equations for blade deformation are then partial differential equations (in time t and span wise coordinate s) instead of the ode's that arise from a hinge model.

These pde's are strongly coupled with a number of ode's for the rigid body types of motion such as rotor azimuth angle, teeter angle, etc. Also a set of ode's can be added to describe the drive train dynamics and the generator behaviour.

3. Kinematics of the rotor blades

3.1 Basic reference frames and transformations

The dynamical equations for the rotor blade are in fact complicated forms of Newton's second law, relating forces to accelerations. There are several techniques available for deriving the equations (see e.g. ref. 1), the Langrangian method being the most widely used (also ref. 2). However, it looses some of its clarity for the case of continuous deformations.

The approach chosen here is to express the acceleration vector of a point on the rotor blade in terms of the discrete and continuous dof's. To be able to apply Newton's law, the acceleration has to be defined in an inertial reference system. This leads to a number of transformations, as described in the present chapter. The technique chosen lends itself very well to computer manipulation, as will become clear.

For the definition of the position of a point on the rotor, two different axes systems are used, see figure 1. The IJK system is the basic inertial frame, XYZ is attached to the elastically undeformed rotor and moving with it. Between the X direction and the (instantaneous!) rotor shaft direction, there is an angle ϕ_t, the teeter angle. The two directions coincide for a rigid hub. The Y^t axis coincides with the projection of an elastically undeformed rotor blade (blade 1) of the plane normal to X. The Z axis completes a orthogonal, right handed frame with X and Y.

The origin of XYZ is taken at the intersection of the rotor blade axes with the rotor shaft for a rigid hub, or at the teeter hinge position for a teeter hub.

Let $\vec{q}$ be a position vector of a point on the deformed rotor expressed in XYZ coordinates. It can be expressed in terms of IJK (inertial) coordinates, $\vec{P}_{IJK}$, by way of the following transformation:

$$\vec{P}_{IJK} = \begin{pmatrix} 0 \\ 0 \\ h_n \end{pmatrix} + \bar{\bar{S}}_y \left\{ \begin{pmatrix} x_{nod} \\ y_{nod} \\ 0 \end{pmatrix} + \bar{\bar{S}}_{tilt} \left[\begin{pmatrix} d_n \\ 0 \\ 0 \end{pmatrix} + \bar{\bar{S}}_{rot} \bar{\bar{S}}_{teet} \vec{q} \right] \right\} \qquad (1)$$

where:

h_n = hubheight;

x_{nod}, y_{nod} = horizontal tower top translation, decomposed along the rotor shaft projection (x_{nod}) and perpendicular to it;

d_n = distance between tower centre line and XYZ origin measured along rotor shaft;

$\bar{\bar{S}}_y$, $\bar{\bar{S}}_{tilt}$, $\bar{\bar{S}}_{rot}$, $\bar{\bar{S}}_{teet}$ = yaw, tilt, rotor angle and teeter rotation matrices, see appendix.

With the XYZ origin as defined before, (1) can be expressed as:

$$\vec{P}_{IJK} = \vec{P}_{or} + \vec{P}_{rel}$$

$$\vec{P}_{or} = \begin{pmatrix} 0 \\ 0 \\ h_n \end{pmatrix} + \bar{\bar{S}}_y \left[\begin{pmatrix} x_{nod} \\ y_{nod} \\ 0 \end{pmatrix} + \bar{\bar{S}}_{tilt} \begin{pmatrix} d_n \\ 0 \\ 0 \end{pmatrix} \right] \qquad (2)$$

$$\vec{P}_{rel} = \bar{\bar{S}}_y \, \bar{\bar{S}}_{tilt} \, \bar{\bar{S}}_{rot} \, \bar{\bar{S}}_{teet} \, \vec{q}$$

3.2 Description of the elastically deformed rotor

In the present section, the expression for $\vec{q}$ will be obtained in terms of elastical deformation functions. First, a number of blade vectors are introduced (figure 2):

$\vec{a}$: along the flexural axis of the blade, supposed to be a straight line;

$\vec{b}$: $\perp \vec{a}$, in the plane defined by $\vec{a}$ and $\vec{X}$, in flap direction;

$\vec{c}$: $\vec{a} \times \vec{b}$ (lag direction).

Distance along the flexural axis will be denoted by s. Figure 3 shows a section of the blade, $\perp \vec{a}$, constant s. In this section x measures distance along the profile chord, θ is the local angle of the undeformed blade between the chord and the rotor plane, and δ is the torsional elastic deformation angle. The figure shows how θ is composed of a fixed (twist) part and a variable (pitch) part, and the sign convention used. Finally, u and v denote elastic deformation in $\vec{b}$ (flap) and $\vec{c}$ (lag) direction respectively.

Mass is supposed to be concentrated along the chord line. The position vector $\vec{q}$ of a point on the chord can then be expressed by:

$$\vec{q} = f(s,u,v)\,\vec{a} + \{u + x \sin(\theta-\delta)\}\,\vec{b} + \{v + x \cos(\theta-\delta)\}\,\vec{c}$$

with: (3)

$$f(s,u,v) = \int_0^s \left[1 - \left(\frac{\partial u}{\partial s}\right)^2 - \left(\frac{\partial v}{\partial s}\right)^2\right]^{1/2} ds$$

Through the function f(s,u,v), the expression includes the effects of reduced 'radial' position due to elastic deformation. The blade vectors $\vec{a}$, $\vec{b}$ and $\vec{c}$ can be expressed as:

$$\vec{a} = \begin{pmatrix} \sin \alpha_c \\ \cos \alpha_c \cos \phi_b \\ \cos \alpha_c \sin \phi_b \end{pmatrix}, \quad \vec{b} = \begin{pmatrix} \cos \alpha_c \\ -\sin \alpha_c \cos \phi_b \\ -\sin \alpha_c \sin \phi_b \end{pmatrix}, \quad \vec{c} = \begin{pmatrix} 0 \\ \sin \phi_b \\ -\cos \phi_b \end{pmatrix} \qquad (4)$$

if α_c denotes the rotor cone angle, and ϕ_b the blade position angle ($\phi_b \stackrel{c}{=} 0$ for blade 1).

3.3 Velocities and accelerations

Substitution of $\vec{q}$ from (3) into (1) or (2) gives the IJK components of the relevant point. The absolute acceleration is obtained by differentiating $\vec{P}$ twice with respect to time. This implies differentiation with respect of all functions of time contained in $\vec{P}$, viz. the degrees of freedom, which shall be denoted by χ_i, i = 1 ... k. In doing so it is important to note that the $\vec{P}$ vector for a given point depends on local values of the 'continuous' dof's u and v but also on integrated values of ∂u/∂s and ∂v/∂s, through f. Although not a separate degree of freedom, it is convenient to treat f as such in the formal expressions for the derivates. Then, the number of dof's is augmented by one, but $\vec{P}$ depends only on local values.

The acceleration vector $d^2\vec{P}/dt^2$ can be expressed as:

$$\frac{d^2\vec{p}}{dt^2} = \sum_j \sum_i \frac{\partial^2 \vec{P}_{or}}{\partial \chi_i \partial \chi_j} \frac{\partial \chi_i}{\partial t} \frac{\partial \chi_j}{\partial t} + \sum_i \frac{\partial \vec{P}_{or}}{\partial \chi_i} \frac{\partial^2 \chi_i}{\partial t^2} +$$

$$\sum_j \sum_i \frac{\partial^2 \vec{P}_{rel}}{\partial \chi_i \partial \chi_j} \frac{\partial \chi_i}{\partial t} \frac{\partial \chi_j}{\partial t} + \sum_i \frac{\partial^2 \vec{P}_{rel}}{\partial \chi_i} \frac{\partial^2 \chi_i}{\partial t^2} \qquad (5)$$

The second part, $d^2\vec{P}_{rel}/dt^2$, shall be worked out further here. It is clear that the j, i summation term is symmetrical with respect to j and i. The expression for $d^2\vec{P}_{rel}/dt^2$ can be written somewhat more condensed as:

$$\frac{d^2\vec{P}_{rel}}{dt^2} = \sum_{j=i}^{K} \sum_{i=1}^{K} (2 - \delta_{ij}) \vec{A}_{ij} \frac{\partial \chi_i}{\partial t} \frac{\partial \chi_j}{\partial t} + \sum_{j=1}^{K} \vec{B}_j \frac{\partial^2 \chi_j}{\partial t^2}$$

with, according to (2):

$$\vec{B}_j = \frac{\partial}{\partial \chi_j} (\bar{\bar{S}}_y \bar{\bar{S}}_{tilt} \bar{\bar{S}}_{rot} \bar{\bar{S}}_{teet} \vec{q}) \qquad (6)$$

$$\vec{A}_{ij} = \frac{\partial}{\partial \chi_i} \vec{B}_j$$

and:

δ_{ij} is the Kronecker δ symbol.

Note that for (χ_i or χ_j) = (u or v), $\vec{A}_{ij}$ = 0, since $\vec{q}$ depends linearly on u and v.

4. Dynamic equations

4.1 Rotational degrees of freedom

The dynamical equations for the dof's concerning rotation can best

be expressed in terms of the angular momentum about the relevant axis. First, a point is selected on the axis of rotation, with respect to which the angular momentum vector is defined. For the rotor azimuth angle or teeter motion, the XYZ origin is a convenient point. The relative linear momentum of a mass element at x,s on the rotor blade is:

$$\delta\vec{i}_{rel} = \rho dx ds \frac{d\vec{P}_{rel}}{dt} \tag{7}$$

ρ = mass density in kg/m^2, as function of x and s.

The relative angular momentum of this element equals:

$$\delta\vec{h}_{rel} = \vec{P}_{rel} \times (\rho dx ds \frac{d\vec{P}_{rel}}{dt}) \tag{8}$$

if x denotes a vectorial 'cross' product. Manipulation of the expression for $d\delta\vec{h}_{rel}/dt$, following ref. 1, section 1.4, gives after application of Newton's law:

$$\frac{d}{dt}\delta\vec{h}_{rel} = \rho dx ds \, \vec{P}_{rel} \times \frac{d^2\vec{P}_{rel}}{dt^2}$$

$$= \vec{P}_{rel} \times \delta\vec{F} - \rho dx ds \, \vec{P}_{rel} \times \frac{d^2\vec{P}_{or}}{dt^2} \tag{9}$$

where $\delta\vec{F}$ is the net 'external' force on the mass element, seen from the inertial reference system.

Integration over the entire rotor structure gives the equation for the rate of change of the (relative) rotor angular momentum:

$$\frac{d}{dt}\vec{h}_{rel} = \iint_{sx} \{\rho dx ds \, \vec{P}_{rel} \times \frac{d^2\vec{P}_{rel}}{dt^2}\} = \vec{Q} - M_{rot}\,\vec{r}_{cg} \times \frac{d^2\vec{P}_{or}}{dt^2} \tag{10}$$

with:
$\vec{Q}$ = total external torque vector, including the mainshaft torque;
M_{rot} = total rotor mass = $\iint \rho dx ds$;
$\vec{r}_{cg}$ = position vector of rotor centre of gravity with respect to $\vec{P}_{or}$.

The equation for the rotor azimuth or teeter dof is obtained by taking the appropriate component of (10), i.e. by taking the dot product of (10) with the rotor shaft direction:

$$\bar{\bar{S}}_y \, \bar{\bar{S}}_{tilt} \begin{matrix}(1)\\(0)\\(0)\end{matrix}$$

or the teeter axis direction, respectively.

For the tilt or yaw degree of freedom the same procedure can be followed, but with respect to the point $(0,0,h_n)$ instead of $\vec{P}_{or}$. For rotor blade torsional deformation, only the x-integral is applied, and $\vec{Q}$ includes the 'internal' beam torsional moments.

By way of the x-integral of the $\vec{P}_{rel} \times \frac{d^2\vec{P}_{rel}}{dt^2}$ product in (10), the following quantities enter the equation:

$m(s) = \int \rho dx$; mass density of the section

$m(s)x_{cg} = \int \rho x dx$; x_{cg} = chordwise position of sectional center of gravity

$m(s)r_\delta^2 = \int \rho x^2 dx$; sectional inertial moment.

These quantities are ordinarilly used in aeroelastic analysis. Their values in function of s should by supplied by the user.

4.2 Elastic bending equations

The fundamental expression for flap and lag motion is Newton's second law relating the relevant component of the acceleration of a beam element to the net force component in that direction. Referring to figure 3, the flap equation is:

$$\int_x \rho dx \frac{d^2\vec{P}_{rel}}{dt^2} \cdot \vec{b} = \frac{dS_f}{ds} + (\int \rho dx)\, \vec{g} \cdot \vec{b} + dF_f/ds \qquad (11)$$

and equivalently for the lag motion (dot product with $\vec{c}$). In (11),

S_f = shear force in flap direction

$m(s)\, \vec{g} \cdot \vec{b}$ = gravitational contribution

$\frac{dF_f}{ds}$ = external (aerodynamic) flap force/m.

The acceleration term $\frac{d^2\vec{P}}{dt^2} \cdot \vec{b}$ contains $\partial^2 u/\partial t^2$, but also all other 'mass' force components in $\vec{b}$ direction.

Following ref. 1, section 9.1, the term dS_f/ds can be worked out for the slender beam theory in terms of $\partial^2 u/\partial s^2$ and other terms, to yield:

$$\frac{\partial^2}{\partial s^2}\left[EI_{ff} \frac{\partial^2 u}{\partial s^2} + EI_{lf} \frac{\partial^2 v}{\partial s^2}\right] - \frac{\partial}{\partial s}\left(G \frac{\partial u}{\partial s}\right) + \int_x \rho dx \frac{d^2\vec{P}}{dt^2} \cdot \vec{b} - m(s)\vec{g} \cdot \vec{b}$$

$$= dF_f/ds \qquad (12)$$

Here the term in square brackets expresses the internal flap wise bending moment (including lag bending coupling), and the term $\frac{\partial}{\partial s}\left(G \frac{\partial u}{\partial S}\right)$ is commonly referred to as 'centrifugal stiffening'. G is the tensile force, which is obtained from equilibrium in $\vec{a}$ direction:

$$G = -\int_s^R \left[\int_x \rho dx \frac{d^2\vec{P}}{dt^2} \cdot \vec{a} - m(s)\vec{g} \cdot \vec{a}\right] ds \qquad (13)$$

The most important contribution to G usually comes from the centripetal acceleration:

$$-m(s)\left(\frac{d\Phi_r}{dt}\right)^2 f(s,u,v),\ \Phi_r \text{ being the rotor azimuth angle.}$$

4.3 Total system of dynamical equations

The procedure described above results in one differential equation for each degree of freedom to be resolved. These equations, together with appropriate initial conditions and boundary conditions (for the pde's), can be solved numerically as will be described in section 5. The equations are strongly coupled; most of the coupling terms come from the acceleration terms as detailed in section 3.

5. Numerical techniques

5.1 Discretization of the derivatives

The dynamical equations for the dof's are solved numerically by finite difference techniques involving discretization of the space and time derivatives. For the latter, an implicit finite difference formulation of second order is chosen. If $t_i = i\Delta t$ is the time for which the state of the system is to be calculated, then time derivates of a quantity ϕ are approximated by:

$$\left.\frac{\partial\phi}{\partial t}\right|_i = \frac{3\phi_i - 4\phi_{i-1} + \phi_{i-2}}{2\Delta t} = D_1\phi_i \tag{14}$$

$$\left.\frac{\partial^2\phi}{\partial t^2}\right|_i = \frac{2\phi_i - 5\phi_{i-1} + 4\phi_{i-2} - \phi_{i-3}}{\Delta t^2} = D_2\phi_i \tag{15}$$

The method is implicit by evaluating all coefficients, including the space derivates, at time t_i. Although this leads to a set of coupled, non-linear algebraic equations, which has to be solved by iteration, the stability characteristics are better than those of explicit schemes.

The characteristics of the scheme can be studied analytically by application to a linear model equation and forming the so-called modified equation. This technique was first introduced by Warming and Hyett (ref. 3) for hyperbolic pde's. It will be applied here to a simple ode, to illustrate the scheme's properties:

$$\frac{d^2x}{dt^2} + 2\xi\,\omega_0\frac{dx}{dt} + \omega_0^2 = \frac{a}{m}\cos ft \tag{16}$$

where ω_0 is the eigenfrequency and the non-dimensional damping.

Using Taylor expansions at t_i, it can be shown that the difference operators D_1 and D_2, defined in (14) and (15), satisfy:

$$D_1 x_i = \frac{dx}{dt}\bigg|_i - \frac{1}{3}\frac{d^3x}{dt^3}\bigg|_i \Delta t^2 + \frac{1}{4}\frac{d^4x}{dt^4}\bigg| t^3 + \ldots$$

$$D_2 x_i = \frac{d^2x}{dt^2}\bigg|_i - \frac{11}{12}\frac{d^4x}{dt^4}\bigg|_i \Delta t^2 + \frac{d^5x}{dt^5}\bigg| \Delta t^3 + \ldots$$

Using (14) and (15) in (16), the 'real' equation solved then is:

$$\frac{d^2x}{dt^2} + 2\xi\,\omega_0 \frac{dx}{dt} + \omega_0{}^2 x - \Delta t^2 \left(\frac{2}{3}\,\xi\,\omega_0 \frac{d^3x}{dt^3} + \frac{11}{12}\frac{d^4x}{dt^4}\right) +$$
$$\Delta t^3 \left[\frac{\xi\omega_0}{2}\frac{d^4x}{dt^4} + \frac{d^5x}{dt^5}\right] + O(\Delta t^4) = \frac{a}{m}\cos ft \qquad (17)$$

The modified equation is now obtained by expressing the derivatives of order 3 and higher in terms of second and first order derivatives, by repeated differentiation of (17). After substantial manipulation, the following result is obtained:

$$\frac{d^2x}{dt^2}\left[1 + \varepsilon^2\left(\frac{11}{12} - \frac{7}{3}\xi^2\right) + \varepsilon^3\xi\left(\frac{7}{2} - 6\xi^2\right) + \ldots\right]$$
$$\frac{dx}{dt}\,2\xi\,\omega_0\left[1 - \frac{7}{12}\varepsilon^2 + \varepsilon^3\left(\frac{1}{2\xi} - \frac{3\xi}{2}\right) + \ldots\right] + \omega_0{}^2 x = \frac{a}{m}\cos ft +$$
$$O\left[\varepsilon^2 \frac{f^2}{\omega_0{}^2}\right]$$

with $\varepsilon = \omega_0\,\Delta t$.

It is clear that accuracy of the scheme is of $O(\omega\Delta t)^2$ (locally). Also, for undamped or slightly damped vibrations, the eigenfrequency of the modified equation will be slightly lower, by a term of $O(\varepsilon^2)$, than that of the original equation. Undamped oscillations of the original equation, $\xi = 0$, are damped in the modified equation by a term of order $\omega_0\,\varepsilon^3$.

Figures 4, 5 and 6 show some results of the numerical solution compared with the analytical one. Figure 4 shows a undamped free vibration solved with $\varepsilon = 0.25$ and 0.1 respectively, illustrating the above observations. Figure 5 shows the results for a damped oscillation with $\xi = 0.1$, will figure 6 shows a forced vibration ($f = 1.5 * \omega_0$) with $\xi = 0.1$. These results indicate that choosing $\varepsilon = 0.1$, a very accurate solution will be obtained, while for many cases $\varepsilon = 0.25$ is still acceptable. The time step to be used should be chosen according to:

$$\Delta t \leq \frac{0.25}{\omega_0}$$

for the highest frequency that the user wants to resolve. If higher frequencies are present in the system, they will be damped numerically.

For the space derivatives, a numerical approximation based on cubic splines is selected. An equidistant grid is defined along the blade axis, with grid points:

$$s_i = i\Delta s,\ i = 0 \ldots N,\ \Delta s = R/N \tag{18}$$

The elastic deformation fields u, v and δ are approximated by a cubic polynomial on each interval $s_i < s < s_{i+1}$, satisfying the conditions that the function and its first two derivatives are continuous on internal grid points s_i, $i = 1 \ldots N-1$.

This approximation is especially suited for an elastic deformation field since deformation, inclination (first derivative) and moment (second derivative) must be continuous functions of s. The third derivative, proportional to the shear force, may be discontinuous.

The equations for elastic deformation, such as (12) are applied at all internal grid points, while the relevant boundary conditions are enforced at s = 0 and s = R (i = 0 and N respectively). In applying the equations, the first and second derivatives of the deformation ϕ (n, v or δ) are replaced by:

$$\left.\frac{\partial\phi}{\partial s}\right|_j = m_{\phi_j} \tag{19}$$

and:

$$\left.\frac{\partial^2\phi}{\partial s^2}\right|_j = M_{\phi_j} \tag{20}$$

where m and M are the spline first and second derivatives respectively. In the u and v equations, higher order derivatives appear, of the form:

$$\frac{\partial^2}{\partial s^2}\left(EI\,\frac{\partial^2\phi}{\partial s^2}\right)$$

which cannot be obtained from the spline representation. These are obtained by central finite differences on M:

$$\left.\frac{\partial^2}{\partial s^2}\left(EI\,\frac{\partial^2\phi}{\partial s^2}\right)\right|_j = \frac{(EI\,M_\phi)_{j+1} - 2(EI\,M_\phi)_j + (EI\,M_\phi)_{j-1}}{\Delta s^2} + O(\Delta s^2) \tag{21}$$

With this procedure, a set of algebraic equations results in terms of ϕ_j, m_{ϕ_j} and M_{ϕ_j}, together with discrete dof's. These equations are combined with the continuity equations for the splines, which have the form (see e.g. ref. 4):

$$\frac{M_{\phi\,j+1} + 4M_{\phi\,j} + M_{\phi\,j-1}}{6} = \frac{\phi_{j+1} - 2\phi_j + \phi_{j-1}}{(\Delta s)^2} \qquad (22)$$

and:

$$\frac{m_{\phi\,j+1} + 4m_{\phi\,j} + m_{\phi\,j-1}}{3} = \frac{\phi_{j+1} - \phi_{j-1}}{\Delta s} \qquad (23)$$

for j = 1 ... N-1.

In fact, (22) and (23) are used to eliminate ϕ_j and $m_{\phi\,j}$ from the equations, and a set of 3N equations results for Mu_j, Mv_j and $M\delta_j$. The solution is obtained in terms of these second derivatives, which (for u and v) are proportional to the bending moments. Shear force and displacement are obtained subsequently using (22) and (23).

Since the equations to be solved are coupled and nonlinear, the system of algebraic equations resulting from the discretization is also nonlinear. It is solved by an iteration process.

5.2 Possibilities for computer manipulation

The most complicated terms in the dynamical equations are the ones expressing the rate of change of linear or angular momentum. In the first case, a scalar product of vectors is involved:

$$\frac{d^2\vec{P}_{rel}}{dt^2} \cdot \vec{\text{direction vector}}$$

in the second case even a vector triple product:

$$\vec{P}_{rel} * \frac{d^2\vec{P}_{rel}}{dt^2} \cdot \vec{\text{direction vector}}$$

Writing out these expressions for a large number of dof's is a considerable effort. Alternative possibilities include the use of a formula manipulator or, the direct numerical evaluation of the matrices, matrix and vector products, etc. Especially this last possibility deserves attention.

Both $\vec{P}_{rel}$ and $d^2\vec{P}_{rel}/dt^2$ can be expressed analytically in condensed form, (2) and (6) with (3). For the numerical evaluation of these vectors it suffices to evaluate numerically the basic transformation matrices and their derivatives, and perform the necessary matrix multiplications. The computer code can then be kept relatively simple, with the least possibility for coding errors.

However, direct numerical evaluation also has some disadvantages. In the first place, the matrices and their derivatives include zero's so that matrix products will involve unnecessary operations like mul-

tiplication with and addition of zero's. Also $\sin^2 + \cos^2$ terms enter, which analytically can be put equal to 1, but require considerable computer time in numerical evaluation.

Secondly, direct numerical evaluation does not add to insight and recognition of the contribution of separate effects. This insight is very valuable in guiding remedial actions in the case of unwanted rotor behaviour.

For these reasons, analytical manipulation of the expressions may be useful, although very labour intensive. In the coding of the PHATAS program, an effort is made to use an intelligent mix of analytical work and direct evaluation. The formulation of the dynamics as presented in this paper, at least offers the possibility of complete direct evaluation, which may constitute an important check on a program also using results of analytic work.

6. Some calculational results

Some results of calculations with the PHATAS-code will be described here. The geometry considered is that of the WEG-MS1 turbine, at Orkney, U.K. This turbine has a diameter of 20 m, and is fitted with a teetered hub. Calculations were performed using a measured windinput signal at three elevations, for a time span of approximately 4 minutes. The calculated time signal for the different qualities was azimuthally binned. Figure 7 shows the flapwise bending moment at 33% blade span, both as calculated and as measured. In the measurements there may be an appreciably offset of the mean due to zero drift of the strain gauges, but the dynamic part should be quite reliable. It can be seen that both the calculated and the measured signal show a pronounced variation with a frequency of 4 times the rotational frequency (4P). This is due to the first blade bending eigenfrequency which happens to be close to 4P. The tower disturbance (periodic) will give an exitation with (among other) 4P contents. The signals do not show a large 1P variation, although there is considerable 1P excitation, due to the vertical windshear and the tower disturbance. However, the teetered hub construction will take out the 1P response.

The azimuthally binned signal of the teeter angle is shown in figure 8. The calculated signal has a $-\cos \phi_r$ like behaviour, having a phase difference of 90° with the $\sin \phi_r$ excitation due to the wind shear. This is theoretically correct, the teeter motion being one of pure 1P resonance, the amplitude of which is only determined by (aerodynamic) damping. Notice however that there is a pronounced phase (and amplitude!) difference between the calculated and measured signals. This is probably due to dynamic inflow effects, which may make the windsignal in the rotorplane lagging with respect to the windsignal upstream. In the near future, a simple model for the wake dynamics will be implemented to investigate the validity if this hypothesis.

The time signal of the flap bending moment has also been Fourier analysed. After filtering the azimuthally binned valves from the original signal, the remaining (stochastic) part has been processed to find the spectral density function (apsd). Figure 9 shows the calcula-

ted and measured apsd. Note that there is little 1P frequency content out more 2P, due to the teetering hub. Also, the 4P (first flapmode) and 7P (2nd flapmode) are cleary present in both measurements and calculations.

The calculations were performed on a Sun3/50 workstation. Computer-time needed is approximately 60 times real time.

7. Conclusions

A simulation model has been made for the dynamic behaviour of a windturbine, based on the (non-linear) equations of motion for the basic degrees of freedom.

The model equations are solved with finite difference techniques on a digital computer.

Calculational results show acceptable agreement with measurements. Better agreement may be expected by introducing unsteady aerodynamic effects, among which the wake dynamics are thought to influence the phase shift of the teeter motion.

8. References

1) Bramwell, A.R.S., Helicopter Dynamics. Edward Arnold Publishers, 1976.
2) Eggleston, D.M. and Stoddard, F.S., Windturbine Engineering Design. Van Nostrand Reinhold Company, NY, 1987.
3) Warming, R.F. and Hyeff, B.J., The modified equation approach to the Stability and Accuracy Analysis of Finite difference methods. J. Comp. Pys. vol. 14, 1974, pp. 159-179.
4) Lindhout, J.P.F., Snel, H. and Merck, W., A fast parabolic module for the solution of MHD channel flow equations between electrode walls. NLR HP 77006 U, 1977.

Acknowledgements

This work was carried out under contract with NOVEM, contract 18.73-083.10. Mr. C. Lindenburg of ECN was of crucial help in modelling the blade equations, and in getting the PHATAS program working.

Appendix A. Transformation matrices

$$\bar{\bar{S}}_y = \begin{vmatrix} \cos\phi_y & -\sin\phi_y & 0 \\ \sin\phi_y & \cos\phi_y & 0 \\ 0 & 0 & 1 \end{vmatrix} \qquad \text{(A-1)}$$

$$\bar{\bar{S}}_{tilt} = \begin{vmatrix} -\cos\alpha_n & 0 & \sin\alpha_n \\ 0 & 1 & 0 \\ -\sin\alpha_n & 0 & -\cos\alpha_n \end{vmatrix} \qquad \text{(A-2)}$$

$$\underline{\underline{S}}_{rot} = \begin{vmatrix} 1 & 0 & 0 \\ 0 & \cos\phi_r & -\sin\phi_r \\ 0 & \sin\phi_r & \cos\phi_r \end{vmatrix} \qquad \text{(A-3)}$$

$$\underline{\underline{S}}_{teet} = \begin{vmatrix} \cos\phi_t & \sin\phi_t \cos\delta_3 & -\sin\phi_t \sin\delta_3 \\ -\sin\phi_t \cos\delta_3 & \cos\phi_t \cos^2\delta_3 + \sin^2\delta_3 & (1-\cos\phi_t)\sin\delta_3 \cos\delta_3 \\ \sin\phi_t \sin\delta_3 & (1-\cos\phi_t)\sin\delta_3 \cos\delta_3 & \cos\phi_t \sin^2\delta_3 + \cos^2\delta_3 \end{vmatrix} \qquad \text{(A-4)}$$

This expression includes the influence of a δ_3 angle in the teeter-hub.

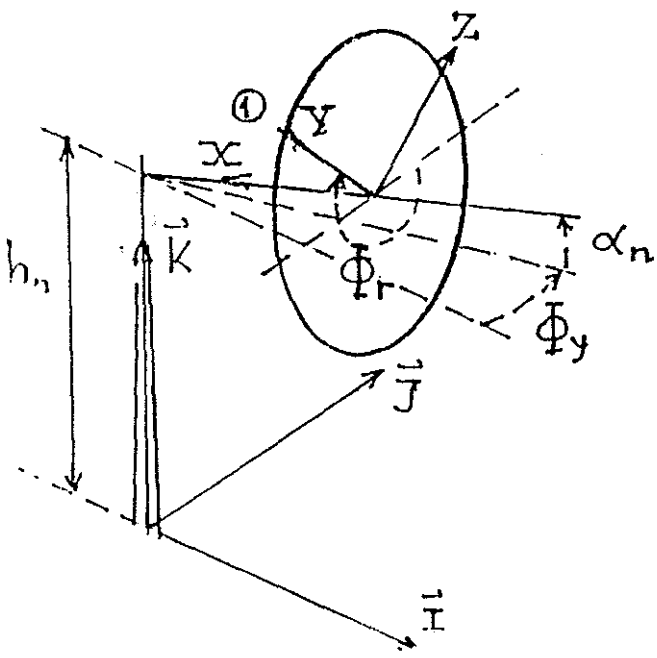

re 1. Definition of basic axes systems.

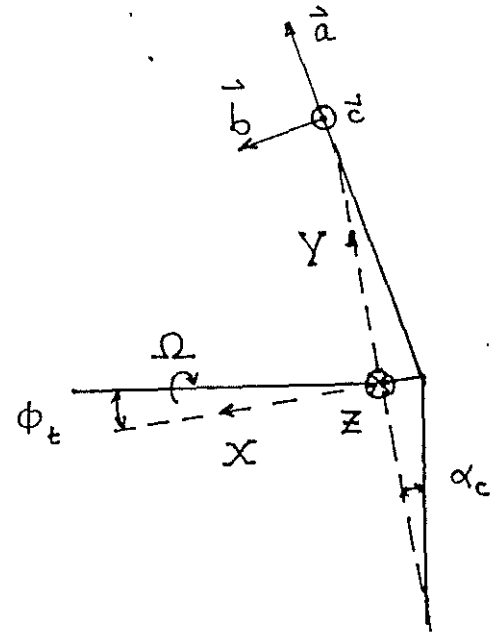

Figure 2. Definition of blade vectors

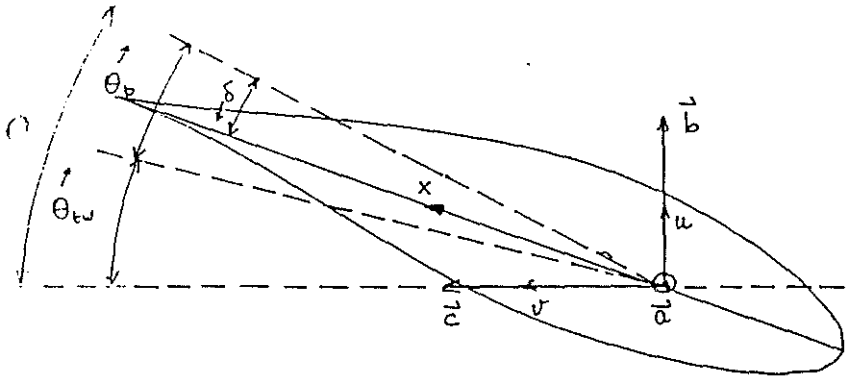

Figure 3. Blade cross section

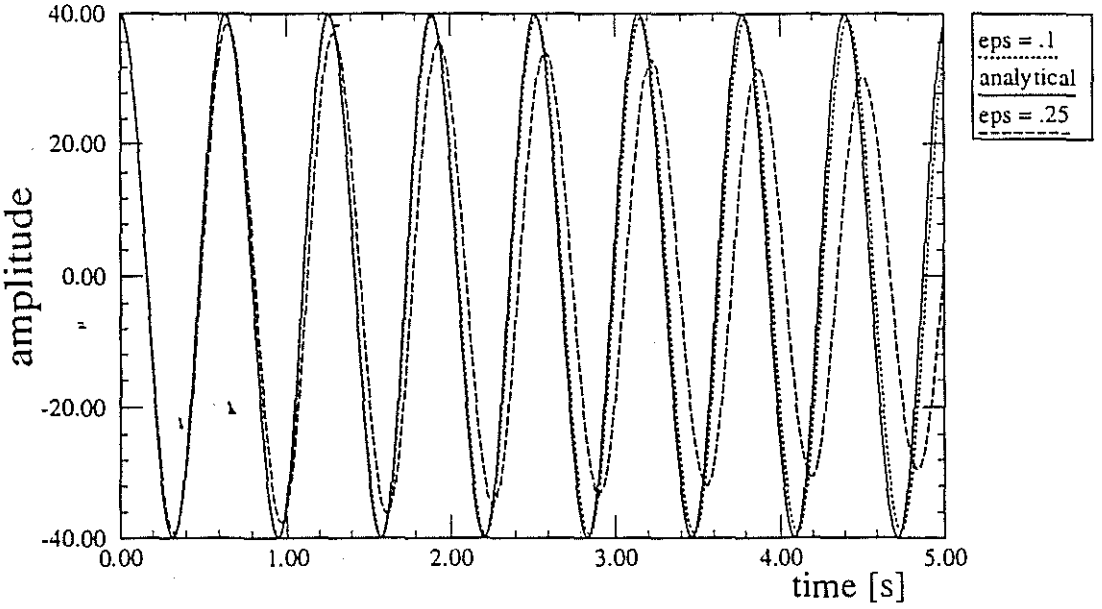

Figure 4. Undamped free vibration, model eq.

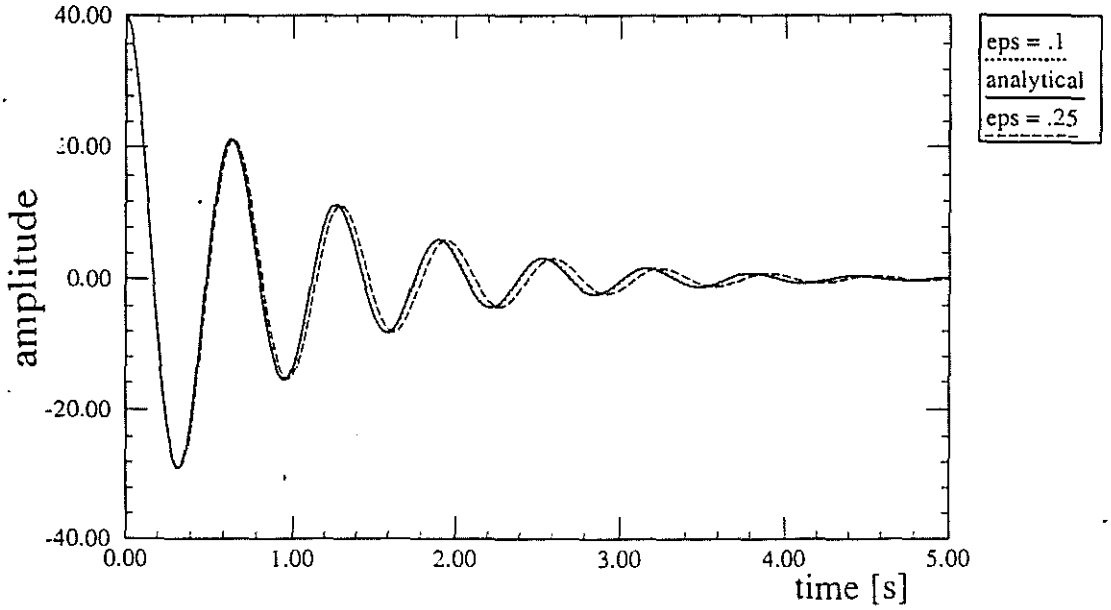

Figure 5. Damped free vibration, model eq. Ksi = .1

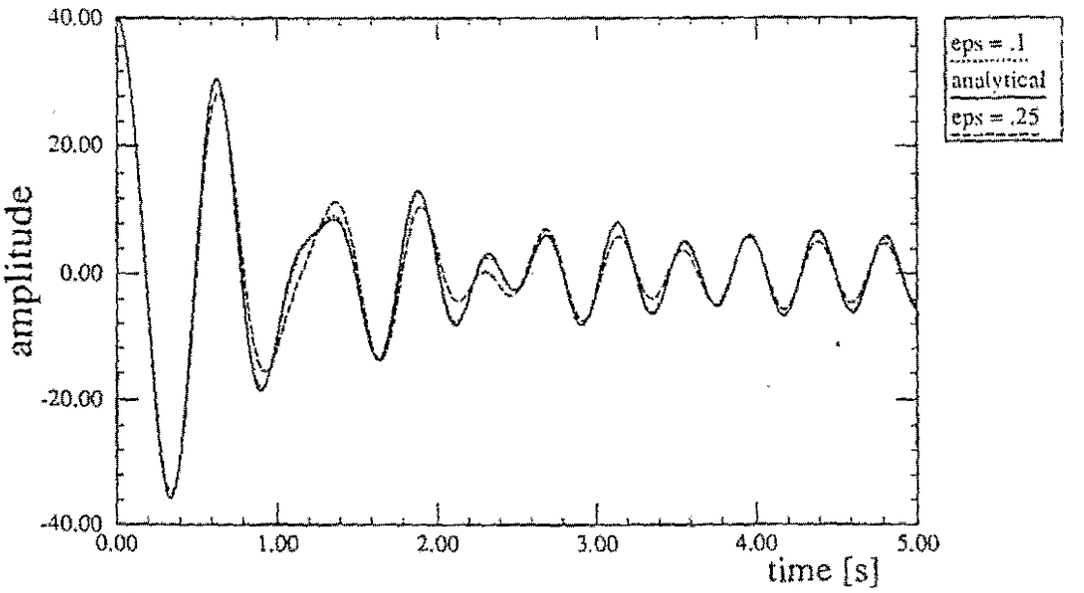

Figure 6. Damped forced vibration, model eq. Ksi = .1

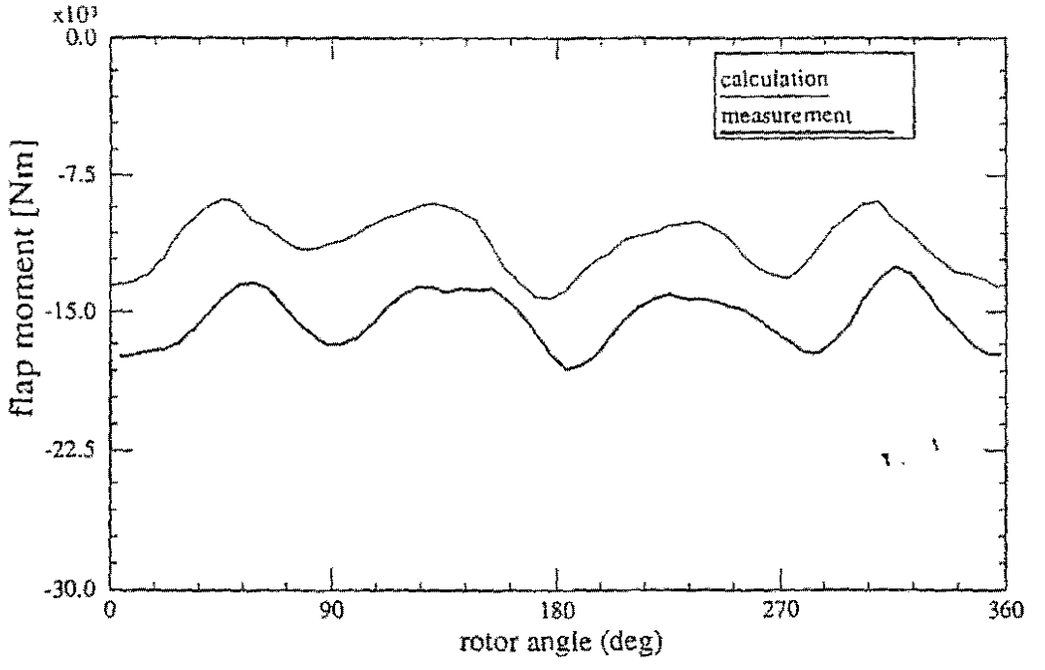

Figure 7. Azimuthally binned flap moment at 33 % span.

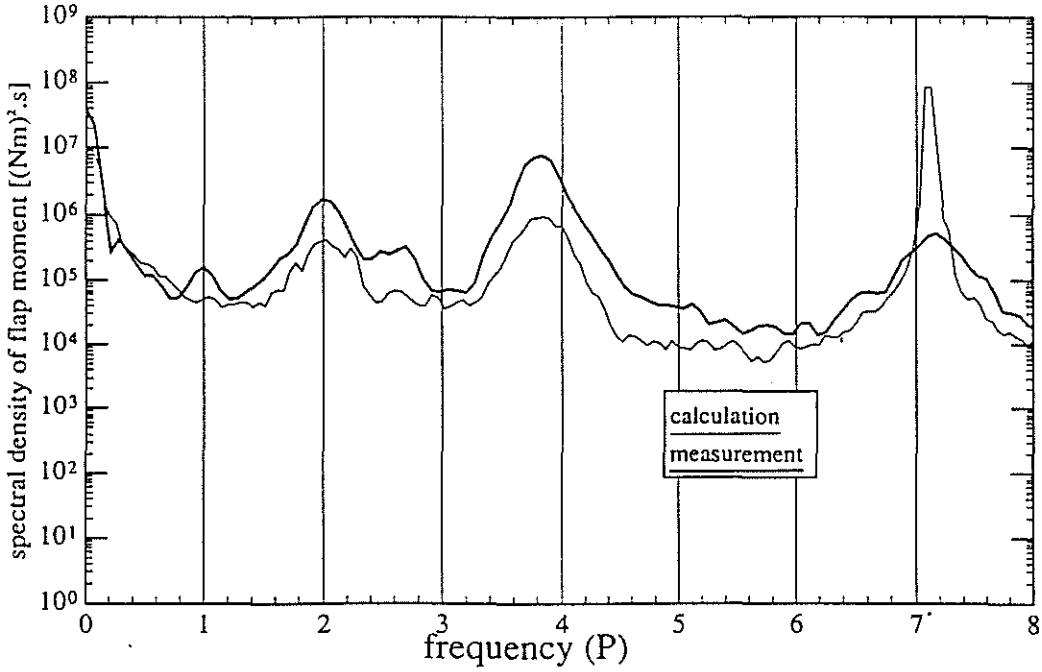

Figure 9. APSD function of flap bending moment

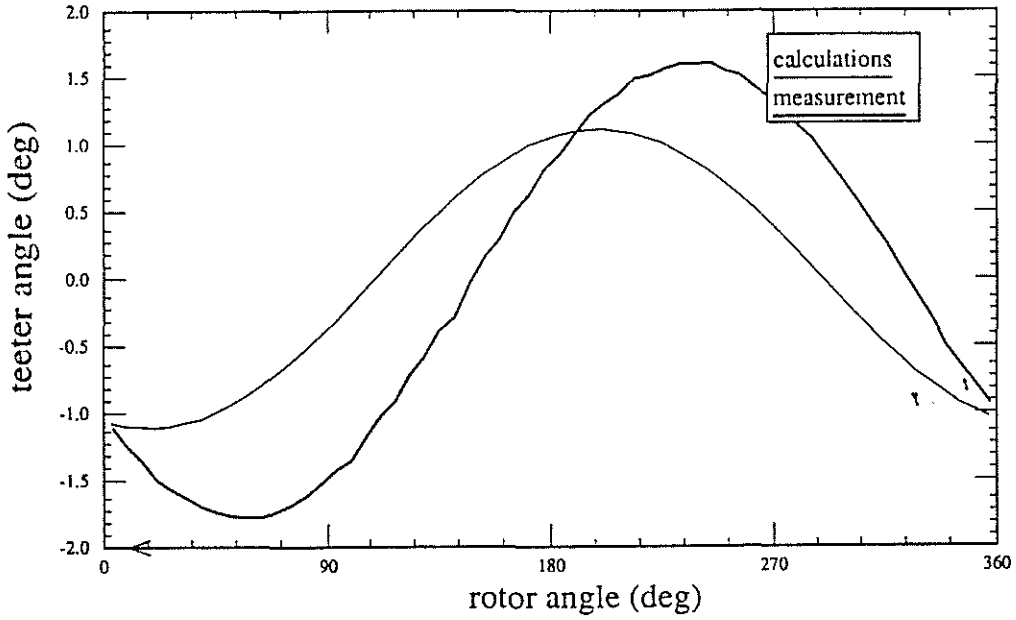

Figure 8. Azimuthally binned teeter angle.